Hidden scalar production at the ILC

Keisuke Fujii[1], Hitoshi Hano[2], Hideo Itoh[1], Nobuchika Okada[1], and Tamaki Yoshioka[2]

1- High Energy Accelerator Research Organization (KEK), Tsukuba, Japan
2- University of Tokyo, International Center for Elementary Particle Physics (ICEPP), Tokyo, Japan

In a class of new physics models, new physics sector is completely or partly hidden, namely, singlet under the Standard Model (SM) gauge group. Hidden fields included in such new physics models communicate with the Standard Model sector through higher dimensional operators. If a cutoff lies in the TeV range, such hidden fields can be produced at future colliders. We consider a scalar filed as an example of the hidden fields. Collider phenomenology on this hidden scalar is similar to that of the SM Higgs boson, but there are several features quite different from those of the Higgs boson. We investigate productions of the hidden scalar at the International Linear Collider (ILC) and study the feasibility of its measurements, in particular, how well the ILC distinguishes the scalar from the Higgs boson, through realistic Monte Carlo simulations.

1 Introduction

In a class of new physics models, a new physics sector is completely or partly singlet under the Standard Model (SM) gauge group, $\mathrm{SU}(3)_C \times \mathrm{SU}(2)_L \times \mathrm{U}(1)_Y$. Such a new physics sector, which we call "hidden sector" throughout this proceedings, includes some singlet fields. These hidden sector fields, in general, couple with the SM fields through higher dimensional operators. If the cutoff scale of the higher dimensional operators lies around the TeV scale, effects of the hidden fields are accessible at future colliders such as the Large Hadron Collider (LHC) and the International Linear Collider (ILC).

There have been several new physics models proposed that include hidden fields. The most familiar example would be the Kaluza-Klein (KK) modes of graviton in extra dimension scenarios [1] [2]. A singlet chiral superfield in the next to Minimal Supersymmetric Standard Model (MSSM) [3] is also a well-known example, which has interesting implications, in particular, on Higgs phenomenology in collider physics [4]. Another example is the supersymmetry breaking sector of the model proposed in Ref. [5], where a singlet scalar field couples with the SM fields through higher dimensional operators with a cutoff around $\Lambda = 1 - 10$ TeV and its collider phenomenology at the LHC and ILC has been discussed. A recently proposed scenario [6], "unparticle physics", also belongs to this class of models. In [7], implications of unparticle on the Higgs phenomenology have been investigated, which have some overlap with what we discuss in the following.

In this proceedings, we present our study on the hidden particle production at the ILC [8]. For simplicity, we introduce a hidden scalar field and assume that the hidden scalar couples with only the SM gauge fields through higher dimensional operators suppressed by a TeV-scale cutoff. In this case, at the ILC, this hidden scalar can be produced through the similar process to the SM Higgs boson production and with the production cross sections comparable to the Higgs boson one. Thus, the hidden scalar production has interesting implications on the Higgs phenomenology. Based on realistic Monte Carlo simulations, we study the feasibility of measurements for the hidden scalar productions and its couplings to

The 8th general meeting of the ILC physics working group, 1/21, 2009

the SM particles, and show how well the hidden scalar can be distinguished from the Higgs boson at the ILC.

2 Hidden particle productions and its decays

We introduce a real scalar field χ as a hidden field, which communicates with the SM sector through interactions of the form,

$$\mathcal{L}_{\rm int} = \frac{c_i}{\Lambda^{d_{\rm SM}-3}} \chi \, \mathcal{O}^i_{\rm SM}, \tag{1}$$

where c_i is a dimensionless coefficient, Λ is a cutoff scale, and $\mathcal{O}^i_{\rm SM}$ is an operator of the SM fields with mass dimension $d_{\rm SM}$. We consider the case that the cutoff, which is naturally characterized by a new physics scale, is around the TeV scale. For a concrete example of this class of models, see Ref. [5].

The theoretical requirements for the SM operator $\mathcal{O}^i_{\rm SM}$ are that it should be a Lorentz scalar operator and be singlet under the SM gauge group. Among many possibilities for such operators, we assume that the hidden scalar couples with only the SM gauge bosons through the operators descried as follows:

$$\mathcal{L}_{\rm int} = -\frac{1}{2} \sum_A \, c_A \, \frac{\chi}{\Lambda} \, {\rm tr} \left[\mathcal{F}^{\mu\nu}_A \mathcal{F}_{A\mu\nu} \right], \tag{2}$$

where c_A is a dimensionless parameter, and $\mathcal{F}_A$'s ($A = 1, 2, 3$) are the field strengths of the corresponding SM gauge groups, U(1)$_Y$, SU(2)$_L$, and SU(3)$_C$. After the electroweak symmetry breaking, Eq. (2) is rewritten as interactions between χ and gluons, photons, Z- and W-bosons.

$$\begin{aligned} \mathcal{L}_{\rm int} = \; & - \; \frac{c_{gg}}{4} \frac{\chi}{\Lambda} G^{a\mu\nu} G^a_{\mu\nu} - \frac{c_{WW}}{2} \frac{\chi}{\Lambda} W^{+\mu\nu} W^-_{\mu\nu} - \frac{c_{ZZ}}{4} \frac{\chi}{\Lambda} Z^{\mu\nu} Z_{\mu\nu} \\ & - \; \frac{c_{\gamma\gamma}}{2} \frac{\chi}{\Lambda} F^{\mu\nu} F_{\mu\nu} - \frac{c_{Z\gamma}}{4} \frac{\chi}{\Lambda} Z^{\mu\nu} F_{\mu\nu}, \end{aligned} \tag{3}$$

where $G^{a\mu\nu}$, $W^{+\mu\nu}$, $Z^{\mu\nu}$ and $F^{\mu\nu}$ are the field strengths of gluon, W-boson, Z-boson and photon, respectively. The couplings c_{gg} etc. can be described in terms of the original three couplings, c_1, c_2 and c_3, and the weak mixing angle θ_w.

The hidden scalar can be produced at the ILC through these interactions. The dominant χ production process is the associated production, $e^+e^- \to \gamma^*, Z^* \to Z\chi$ and $e^+e^- \to \gamma^*, Z^* \to \gamma\chi$. First, let us consider the process $e^+e^- \to Z\chi$. It is interesting to compare this χ production process to the similar process of the associated Higgs production (Higgsstrahlung), $e^+e^- \to Zh$, through the Standard Model interaction $\mathcal{L}_{\rm int} = \frac{m_Z^2}{v} h Z^\mu Z_\mu$. In Figure 1, we show the ratio of the total cross sections between χ and Higgs boson productions as a function of Λ at the ILC with the collider energy $\sqrt{s} = 500$ GeV. Here we have taken $c_1 = c_2$ and $m_\chi = m_h = 120$ GeV. The ratio, $\sigma(e^+e^- \to Z\chi)/\sigma(e^+e^- \to Zh)$, becomes one for $\Lambda_{\rm IR} \simeq 872$ GeV, and it decreases proportionally to $1/\Lambda^2$. Note that in the high energy limit, the χ production cross section becomes energy-independent, as can be understood from the dimension of the interaction terms.

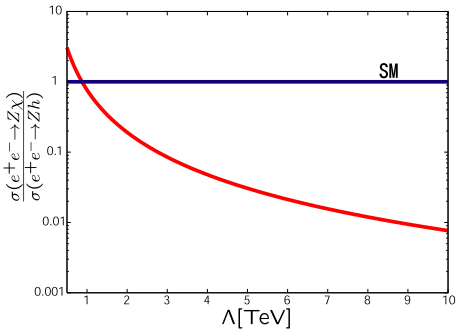

Figure 1: The ratio of total cross sections between the associated χ and Higgs productions as a function of Λ, at the ILC with the collider energy $\sqrt{s} = 500$ GeV. Here, we have fixed the parameters such as $m_\chi = m_h = 120$ GeV and $c_1 = c_2 = 1$. The ratio becomes one for $\Lambda \simeq 872$ GeV.

The coupling manner among χ and the Z-boson pair is different from that of the Higgs boson. As can be understood from Eq. (3), χ couples with the transverse modes of the Z-bosons, while the Higgs boson mainly couples with the longitudinal modes. This fact reflects into the difference of the angular distribution of the final state Z-boson. In the high energy limit, we find $\frac{d\sigma}{d\cos\theta}(e^+e^- \to Z\chi) \propto 1 + \cos^2\theta$, while $\frac{d\sigma}{d\cos\theta}(e^+e^- \to Zh) \propto 1 - \cos^2\theta$. Figure 2 shows the angular distributions of the associated χ and Higgs boson productions, respectively. Even if $m_\chi = m_h$ and the cross sections of χ and Higgs boson productions are comparable, the angular dependence of the cross section can distinguish the χ production from the Higgs boson one.

Next, we consider χ decay processes into a pair of gauge bosons. Figure 3 shows the branching ratio of the χ decay for a special parameter set. We see that the branching ratio of the χ decay is quite different from that of the Higgs boson. In particular, the branching ratio of $\chi \to \gamma\gamma$ can be large, $\mathrm{Br}(\chi \to \gamma\gamma) \simeq 0.1$ for the parameter set in Figure 3. On the other hand, the branching ratio of the Higgs boson into two photons in the SM is at most 10^{-3}, since the coupling between the Higgs boson and two photons are induced through one-loop radiative corrections.

There are several models where the branching ratio of the Higgs boson into two photons is enhanced due to new physics effects. For example, in the MSSM with a large $\tan\beta$ [9], the lightest Higgs boson almost coincides with the up-type Higgs boson of the weak eigenstate. As a result, the Yukawa coupling to bottom quark is suppressed and two-photon branching ratio is relatively enhanced. Another example is the Next to MSSM (NMSSM), where a pseudo scalar (A^0) couples to the lightest (SM-like) Higgs boson. In this model, the Higgs boson can decay into two pseudo scalars ($h \to A^0A^0$) with a sizable branching ratio. If the pseudo scalar is extremely light (lighter than twice the pion mass), it dominantly decays into two photons ($A^0 \to \gamma\gamma$), so that Higgs boson decays into four photons. Since the pseudo-scalar is very light, two photons produced in its decay are almost collinear and will be detected as a single photon [4]. As a result, the Higgs decay into two pseudo-scalars, followed by $A^0 \to \gamma\gamma$, effectively enhances the Higgs branching ratio into two photons [4]. Therefore, the anomalous branching ratio alone is not enough to distinguish such a Higgs boson from χ (in the associated production with a Z-boson) and the measurements of angular distribution and

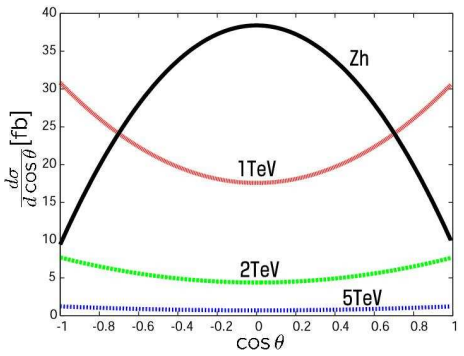

Figure 2: The angular dependence of the cross sections for $m_\chi = m_h = 120$ GeV at the ILC with the collider energy $\sqrt{s} = 500$ GeV and $\Lambda = 1$, 2 and 5 TeV.

polarization of the final state Z-boson are crucial.

There are many possible choices of the parameter set (c_1, c_2 and c_3). In order to simplify our discussion, we choose a special parameter set in the following analysis: $c_1 = c_2 = 1$ and $c_3 = 0$, namely the gluophobic but universal for c_1 and c_2. In this choice, the χ production through the gluon fusion at hadron colliders is closed. For $m_\chi < 2m_W$, the hidden scalar has a 100% branching ratio into two photons.

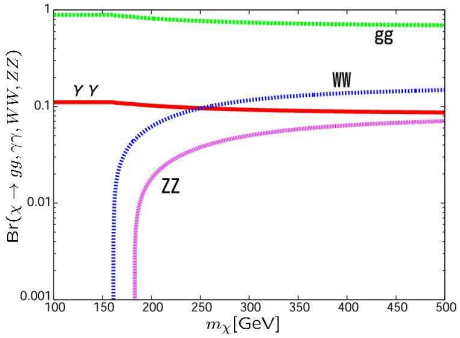

Figure 3: The branching ratio of the hidden scalar (χ) as a function of its mass m_χ. Different lines correspond to the modes, $\chi \to gg$, WW, $\gamma\gamma$ and ZZ.

3 Monte Carlo Simulation

As estimated in the previous section, if the cut-off is around 1 TeV, the production cross section of the hidden scalar can be comparable to the Higgs boson production cross section at the ILC. There are two main production processes associated with a Z-boson or a photon. In the following, we investigate each process. In our analysis, we take the same mass for the hidden scalar and the Higgs boson: $m_\chi = m_h = 120$ GeV, as a reference.

3.1 Observables to be measured

The associated hidden scalar production with a Z-boson is very similar to the Higgs production process and their production cross sections are comparable for $\Lambda \simeq 1$ TeV. One crucial difference is that the hidden scalar couples to Z-bosons through Eq. (3) so that the Z-boson in the final state is mostly transversely polarized. On the other hand, in the Higgs boson production the interaction between the Higgs boson and the longitudinal mode of the Z-boson dominates. In order to distinguish the hidden scalar from the Higgs boson, we will measure

(1) the angular distribution of the Z-boson in the final state,

(2) the polarization of the Z-boson in the final sate.

As shown in the previous section, the branching ratio of the hidden scalar decay is quite different from the Higgs boson one. In our reference parameter set, the hidden scalar decays 100% into two photons. The Higgs boson with $m_h = 120$ GeV dominantly decays into a bottom and anti-bottom quark pair. In order to distinguish the hidden scalar from the Higgs boson, we will measure

(3) the branching ratios into two photons and into the bottom and anti-bottom quark pair through b-tagging.

The associated hidden scalar production with a photon is unique and such a process for the Higgs boson is negligible. We will investigate similar things as in the Z-boson case.

3.2 Analysis Framework

For Monte Carlo simulation studies of the hidden scalar productions and decays, we have developed event generators of the processes: $e^+e^- \to \gamma\chi$ and $e^+e^- \to Z\chi$ followed by

the $\chi \to \gamma\gamma$ decay, which are now included in `physsim-2007a` [11]. In the helicity amplitude calculations, we retain the Z-boson wave function if any and replace it with the wave function composed with the daughter fermion-antifermion pair according to the HELAS algorithm [12]. This allows us to properly take into account the gauge boson polarization effects. The phase space integration and generation of parton 4-momenta are performed with `BASES/SPRING` [13]. Parton showering and hadronization are carried out using `PYTHIA6.3` [14] with final-state tau leptons treated by `TAUOLA` [15] in order to handle their polarizations properly. The background $e^+e^- \to Zh$ events are generated using the $e^+e^- \to Z\chi$ generator with the $e^+e^- \to Z\chi$ helicity amplitudes replaced by corresponding $e^+e^- \to Zh$ amplitudes and the Higgs decay handled by `PYTHIA6.3`.

In the Monte Carlo simulations, we set the nominal center-of-mass energy at 500 GeV and assume no beam polarization. Effects of natural beam-energy spread and beamstrahlung are taken into account according to the beam parameters given in [16]. We have assumed no crossing angle between the electron and the positron beams and ignored the transverse component of the initial state radiation. Consequently, the $Z\chi$ or $\gamma\chi$ system in our Monte-Carlo sample has no transverse momentum.

The generated Monte-Carlo events were passed to a detector simulator (`JSF Quick Simulator` [17]) which incorporates the ACFA-LC study parameters (see Table. 1). The quick simulator created vertex-detector hits, smeared charged-track parameters in the central tracker with parameter correlation properly taken into account, and simulated calorimeter signals as from individual segments, thereby allowing realistic simulation of cluster overlapping. It should also be noted that track-cluster matching was performed to achieve the best energy-flow measurements.

Detector	**Performance**	**Coverage**
Vertex detector	$\sigma_{\rm b} = 7.0 \oplus (20.0/p)\ /\ \sin^{3/2}\theta\ \mu$m	$\lvert\cos\theta\rvert \leq 0.90$
Central drift chamber	$\sigma_{p_T}/p_T = 1.1 \times 10^{-4} p_T \ \oplus\ 0.1\ \%$	$\lvert\cos\theta\rvert \leq 0.95$
EM calorimeter	$\sigma_E/E = 15\ \%/\sqrt{E}\ \oplus 1\ \%$	$\lvert\cos\theta\rvert \leq 0.90$
Hadron calorimeter	$\sigma_E/E = 40\ \%/\sqrt{E}\ \oplus 2\ \%$	$\lvert\cos\theta\rvert \leq 0.90$

Table 1: ACFA study parameters for an LC detector, where p, p_T, and E are measured in units of GeV.

3.3 Event Selection and Results

3.3.1 $e^+e^- \to Z\chi; \chi \to \gamma\gamma$ process

Data equivalent to 50 fb^{-1} have been generated for both $e^+e^- \to Z\chi$ followed by $\chi \to \gamma\gamma$ and $e^+e^- \to Zh$ followed by $h \to \gamma\gamma$. A typical event is displayed in Figure 4. For the $Z\chi \to q\bar{q}\gamma\gamma$ process, there are two jets and two photons in the final state. In the event selection, it is firstly required that the number of reconstructed particles ($N_{particles}$) is greater than 4. In the next, the number of photons reconstructed in the calorimeters (N_{gammas}) is greater than 2, and the two photons whose invariant mass is the closest to m_χ are selected. Finally, the number of jets (N_{jets}) is required to be equal to 2. These selection criteria are summarized in Table 2 together with efficiency of each cut. The distribution of the invariant mass of the two photons which are considered to come from a χ decay is shown

in Figure 5 after imposing all the above selection criteria. In the figure, the grey histogram is for the $e^+e^- \to Zh$ process where the number of remaining events is much less than that of the $e^+e^- \to Z\chi$ process. Figures 6 and 7 show the χ and Higgs production angles (left) and the angular distribution of the reconstructed jets from associated Z-boson decays (right) for the both processes, respectively. As can be seen from these plots, χ couples with the transverse modes of the Z-bosons, while the Higgs boson couples with the longitudinal modes. The $e^+e^- \to Zh$ followed by $h \to A^0A^0$ process is also analyzed with the same cut conditions and its cut statistics is summarized in Table 2. Here, we have assumed $\mathrm{Br}(h \to A^0A^0) = 0.1$ and $\mathrm{Br}(A^0 \to \gamma\gamma) = 1$. The distribution of the invariant mass of the two photons will be similar to Figure 5 in this model, but again we can discriminate the χ from the Higgs by looking at the angular distributions. Figure 8 shows the Higgs production angle and the angular distribution of the reconstructed jets from associated Z-boson decays (right) for the $h \to A^0A^0$ process.

Cut	$Z\chi; \chi \to \gamma\gamma$	$Zh; h \to \gamma\gamma$	$Zh; h \to A^0A^0$
No Cut	2187 (1.0000)	142 (1.000)	7087 (1.0000)
$N_{particles} \geq 4$	1738 (0.7947)	106 (0.747)	5692 (0.8032)
$N_{gammas} \geq 2$	1521 (0.8751)	96 (0.906)	4865 (0.8547)
Cut on $M_{\gamma\gamma}$	1499 (0.9855)	95 (0.990)	4828 (0.9924)
$N_{jets} = 2$ for Ycut $= 0.004$	1498 (0.9993)	95 (1.000)	4825 (0.9994)
Total Efficiency	0.6850 ± 0.0099	0.669 ± 0.040	0.6808 ± 0.0055

Table 2: Cut statistics and breakdown of selection efficiency. The numbers inside and outside of parenthesis are the efficiency and the remaining number of events after each cut, respectively.

3.3.2 $e^+e^- \to \gamma\chi; \chi \to \gamma\gamma$ process

Data equivalent to 5.7 fb^{-1} have been generated for both signal ($e^+e^- \to \gamma\chi$ followed by $\chi \to \gamma\gamma$) and background ($e^+e^- \to \gamma\gamma$ with an ISR photon) processes. A typical signal event is displayed in Figure 9. For the $\gamma\chi \to \gamma\gamma\gamma$ process, there are three photons in the final state. The number of photons reconstructed in the calorimeters (N_{gammas}) is required to be equal to 3. It is also required that the energy and the cosine of the polar angle of each photon are greater than 1 GeV and less than 0.999, respectively. Among the photons, two photons whose invariant mass is within $m_\chi \pm 25$ GeV are considered to be from a χ decay. Finally, the cosines of the production angles of both χ and the remaining photon are required to be less than 0.99. These selection criteria are summarized in Table 3 together with their efficiencies. The distribution of the invariant mass of two photons which are considered to come from a χ decay (left) and the angular distribution of the χ (right) are shown in Figure 10 after imposing all the above selection criteria. A peak at m_χ can be clearly seen over the grey background histogram with the angular distribution consistent with $1 + \cos^2\theta$.

Cut	$\gamma\chi; \chi \to \gamma\gamma$	$\gamma\gamma$ with an ISR
No Cut	600 (1.0000)	100000 (1.0000)
$N_{gammas} = 3$	575 (0.9583)	3746 (0.0375)
$E_{gamma} > 1$ GeV	575 (1.0000)	3730 (0.9959)
$\lvert\cos(\theta_j)\rvert \leq 0.999$	575 (1.0000)	3728 (0.9992)
$\lvert M_{\gamma\gamma} - m_\chi\rvert \leq 25$ GeV	573 (0.9965)	1332 (0.3573)
$\lvert\cos(\theta_\chi)\rvert$ and $\lvert\cos(\theta_a)\rvert \leq 0.99$	572 (0.9983)	1269 (0.9529)
Total Efficiency	0.9533 ± 0.0086	0.0127 ± 0.0001

Table 3: Similar to Table 2 for $e^+e^- \to \gamma\chi$ and $e^+e^- \to \gamma\gamma$ with an ISR photon.

4 Summary and discussions

If a hidden scalar field appears in a certain class of new physics models around the TeV scale, there are interesting implications for collider phenomenology. In particular, since the scalar behaves like the Higgs boson in its production process, it is an interesting issue how to distinguish the scalar from the Higgs boson in future collider experiments. We investigated the hidden scalar production at the ILC and addressed this issue based on realistic Monte Carlo simulations.

With the χ production cross section comparable to the Higgs boson one, the invariant mass distribution reconstructed from two-photon final states due to the decay mode $\chi \to \gamma\gamma$ shows a clear peak at m_χ. In the χ production associated with a Z-boson, the χ production angle and the angular distribution of the reconstructed jets from the associated Z-boson decay reveal that the hidden scalar couples to transversally polarized Z-bosons. On the other hand, the Higgs boson production associated with a Z-boson shows clearly different results in angular distributions and distinguishable from the hidden scalar production.

We have concentrated on the hidden scalar production associated with a Z-boson or a photon. It is also interesting to investigate the weak boson fusion process. For example, in the Z-boson fusion process, measuring the correlations between the cross section and the azimuthal angle between the final state electron and positron can be used to distinguish the couplings between a scalar and the Z-boson with different polarizations.

5 Acknowledgments

The authors would like to thank all the members of the ILC physics subgroup [18] for useful discussions and comments. This study is supported in part by the Creative Scientific Research Grant No. 18GS0202 of the Japan Society for Promotion of Science.

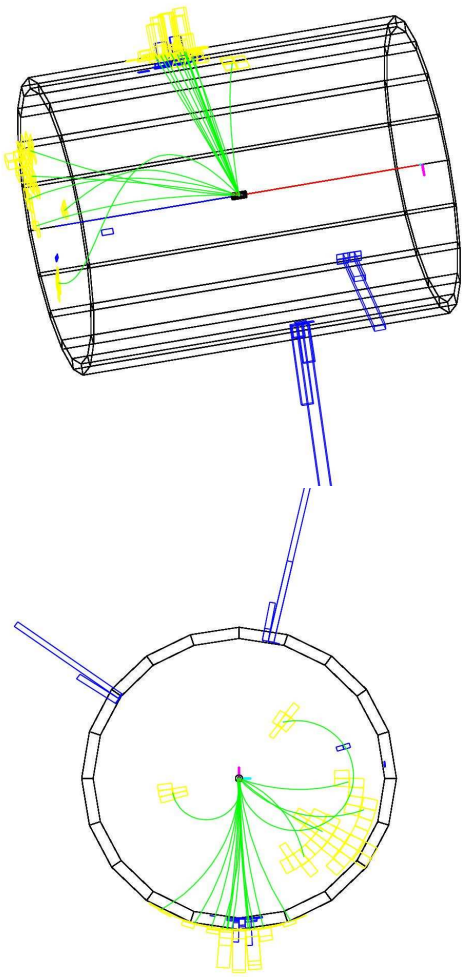

Figure 4: Event displays of $e^+e^- \to Z\chi$ followed by $\chi \to \gamma\gamma$. Two jets from the Z-boson decay and two photons from the χ decay can be clearly seen.

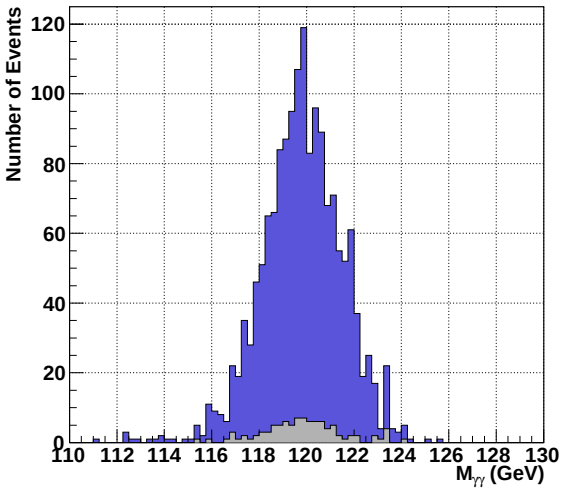

Figure 5: The distribution of the invariant mass of two photons which are considered to come from a χ decay.

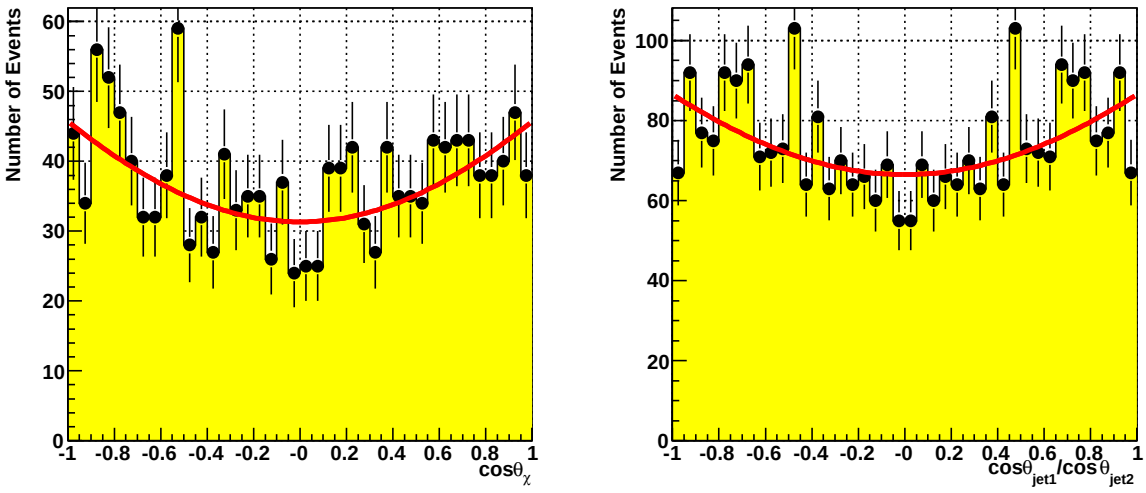

Figure 6: The χ production angle (left) and the angular distribution of the reconstructed jets from associated Z-boson decays (right).

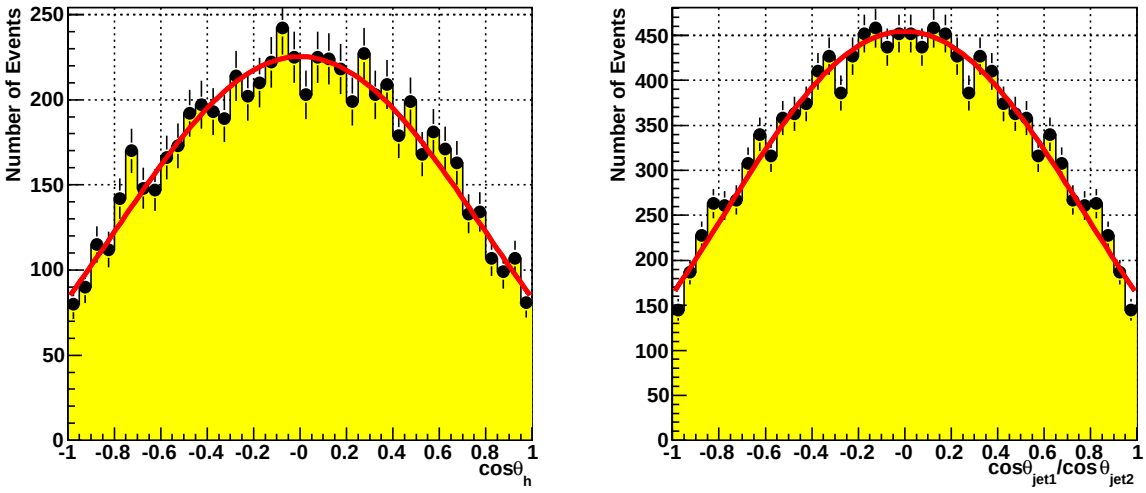

Figure 7: The Higgs production angle (left) and the angular distribution of the reconstructed jets from associated Z-boson decays (right) for $e^+e^- \to Zh$ followed by $H \to \gamma\gamma$.

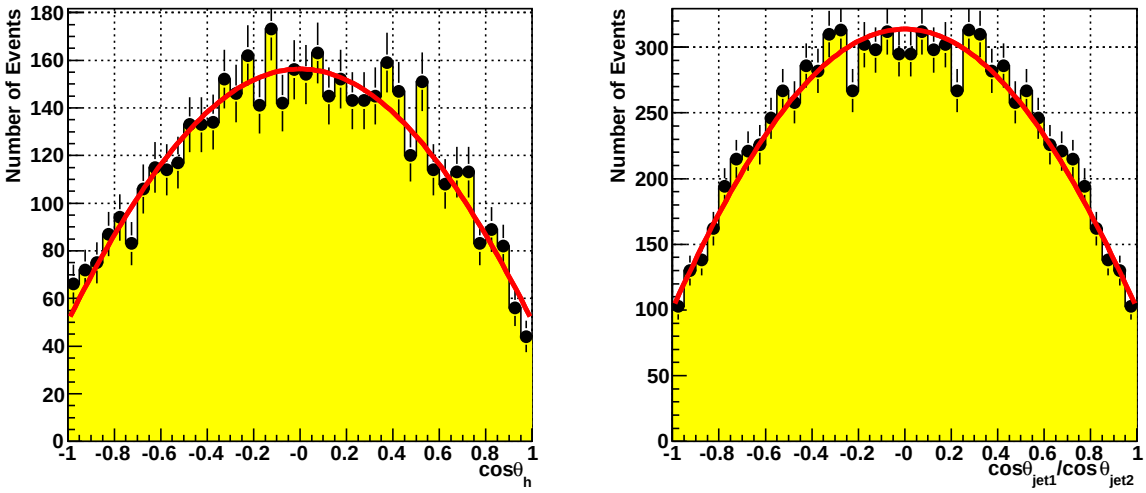

Figure 8: The Higgs production angle (left) and the angular distribution of the reconstructed jets from associated Z-boson decays (right) for $e^+e^- \to Zh$ followed by $h \to A^0A^0$.

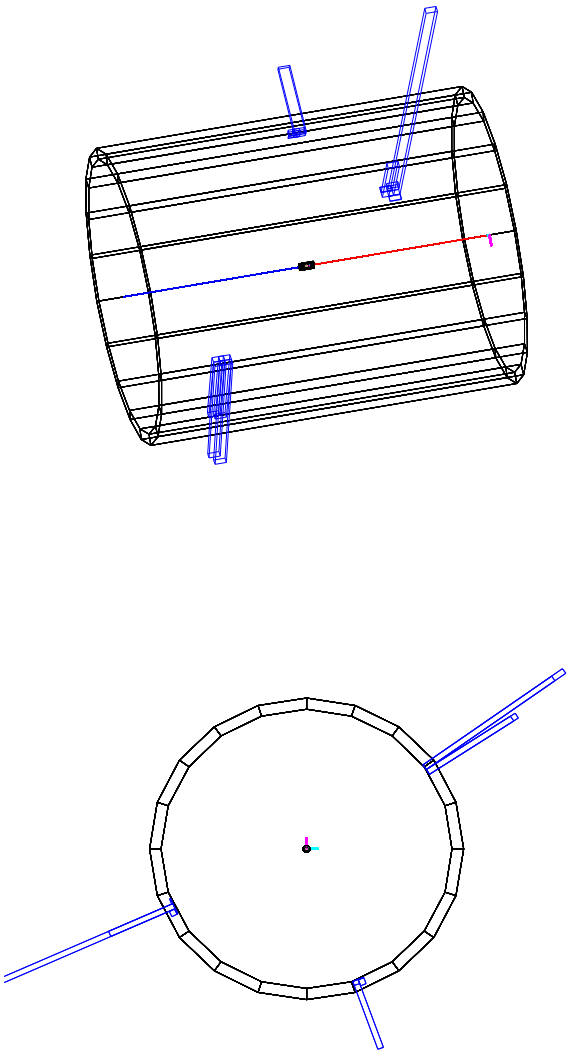

Figure 9: Event displays of $e^+e^- \to \gamma\chi$ followed by $\chi \to \gamma\gamma$.

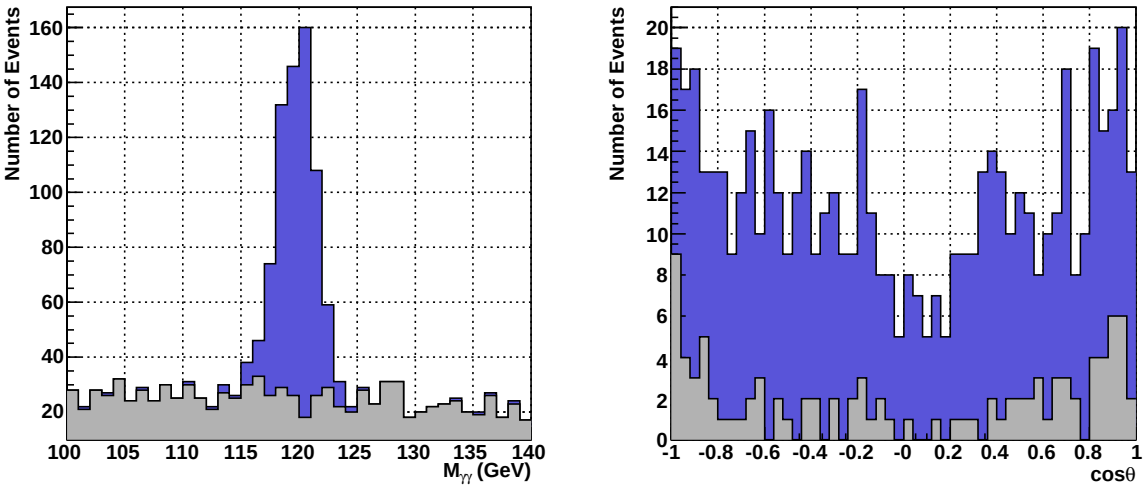

Figure 10: The distribution of the invariant mass of two photons which are considered to come from a χ decay (left) and the angular distribution of the χ (right) for the $e^+e^- \to \gamma\chi$ process with background.

References

[1] N. Arkani-Hamed, S. Dimopoulos and G. Dvali, Phys. Lett. **B429**, 263 (1998); I. Antoniadis, N. Arkani-Hamed, S. Dimopoulos and G. Dvali, Phys. Lett. **B436**, 257 (1998); N. Arkani-Hamed, S. Dimopoulos and G. Dvali, Phys. Rev. **D59**, 086004 (1999).

[2] L. Randall and R. Sundrum, Phys. Rev. Lett. **83**, 3370 (1999).

[3] See, for example, J. F. Gunion, H. E. Haber, G. L. Kane and S. Dawson, *The Higgs Hunter's Guide*, Addison-Weseley: Redwood City, California, 1989.

[4] B. A. Dobrescu, G. L. Landsberg and K. T. Matchev, Phys. Rev. D **63**, 075003 (2001).

[5] H. Itoh, N. Okada and T. Yamashita, Phys. Rev. D **74**, 055005 (2006).

[6] H. Georgi, Phys. Rev. Lett. **98**, 221601 (2007).

[7] T. Kikuchi and N. Okada, Phys. Lett. B **661**, 360 (2008).

[8] K. Fujii, H. Hano, H. Itoh, N. Okada and T. Yoshioka, Phys. Rev. D **78**, 015008 (2008).

[9] H. Baer and J. D. Wells, Phys. Rev. D **57**, 4446 (1998) [arXiv:hep-ph/9710368]; W. Loinaz and J. D. Wells, Phys. Lett. B **445**, 178 (1998) [arXiv:hep-ph/9808287]; M. S. Carena, S. Mrenna and C. E. M. Wagner, Phys. Rev. D **60**, 075010 (1999) [arXiv:hep-ph/9808312]; Phys. Rev. D **62**, 055008 (2000) [arXiv:hep-ph/9907422].

[10] S. Mrenna and J. D. Wells, Phys. Rev. D **63**, 015006 (2000) [arXiv:hep-ph/0001226].

[11] physsim-2007a, `http://www-jlc.kek.jp/subg/offl/physsim/` .

[12] H. Murayama, I. Watanabe and K. Hagiwara, *KEK Report*, 91-11 (1992).

[13] S. Kawabata, *Comp. Phys. Commun.* **41**, 127 (1986).

[14] T. Sjöstrand, L. Lönnblad, S. Mrenna, P. Skands, hep-ph/0308153 (2003).

[15] S. Jadach, Z. Was, R. Decker and J. H. Kühn, *Comp. Phys. Commun.* **76**, 361 (1993).

[16] GLD Detector Outline Document.

[17] JSF Quick Simulator, `http://www-jlc.kek.jp/subg/offl/jsf/` .

[18] http://www-jlc.kek.jp/subg/physics/ilcphys/.